HIGH-RESOLUTION RADIO FREQUENCY INTERFERENCE DETECTION IN MICROWAVE RADIOMETRY USING DEEP LEARNING

A. M. $Alam^{(1)}$, M. $Kurum^{(1)}$, A. C. $Gurbuz^{(1)}$

(1) Mississippi State University, Mississippi State, MS, USA

ABSTRACT

The success of microwave radiometry depends on how accurately it can measure the natural emission of the Earth without the effects of unwanted signals. The consequence of unwanted signals in radiometers is known as radio frequency interference (RFI). The high intensity of these corrupted signals, along with wider bandwidth and longer duration, may jeopardize the overall success of a mission. These reasons resulted in a need for a robust RFI detection algorithm that will enable the mitigation of the contaminated portions of the measurements. Attributes related to RFI could be very dynamic, making it very difficult to detect with a particular algorithm. To address this issue, deep learning (DL) could be an attractive solution to detect RFI with the help of timefrequency analysis, i.e., spectrograms of the received measurement. This study aims to detect and localize RFI in a particular time-frequency bin of spectrograms with the help of DL to retrieve the non-contaminated portion of the measurements.

Index Terms— Microwave Radiometry, SMAP, RFI, Deep Learning, Radiometer

1. INTRODUCTION

Microwave radiometers are designed to measure natural emissions which are very low power. This is essential to measure the earth brightness temperature that helps to map numerous geophysical parameters. This necessitates the importance of designing highly sensitive passive sensors along with protection in the spectrum that is conducted through a guarded bandwidth such as 1400-1427 MHz. These resolutions alone are not enough to limit the effects of radio frequency interference (RFI). Numerous defensive measurements are invented and implemented to equip microwave radiometers to detect RFI and mitigate them from final measurements.

Currently, there are RFI detection approaches available in spaceborne satellites such as NASA's soil moisture active passive (SMAP) [1]. These algorithms such as kurtosis, crossfrequency, and pulse detection, are developed by physical modeling of RFI with a fixed hypothesis. Power level, duty cycle,

and bandwidth can dynamically change the attributes and features of RFI sources, making it very challenging to model the possible outcome to aid detection. Domain transformation is essential for the detection algorithm as it enables them to address different features of RFI. These transformations can be divided into frequency, code, space, polarization, and time. To maximize the performance, multiple domains are aggregated, and among them, the most popular is time-frequency analysis. Although these algorithms are useful for one particular type of RFI, combining different algorithms is critical to increasing efficiency.

Deep learning (DL) has been introduced to coherently detect these different types of RFI with a single algorithm [2,3]. DL-based frameworks in these studies are trained and tested with the spectrograms of NASA's SMAP radiometer raw antenna counts. This method's drawback is that it only identifies RFI at the spectrogram level and decides if a SMAP spectrogram is RFI contaminated or not. If RFI is not detected at a higher resolution featuring the time-bandwidth coverage of RFI within the spectrogram then the entire measurement must be eliminated from the final estimation. Approaches detecting RFI at the spectrogram level might not be well suited for spectrum co-existence and wide-band radiometers where spectrum information is crucial. These factors make it crucial to develop a high-resolution RFI detection method that would aid in robustness and preserve the uncontaminated portion of the data. This study will help to address this issue by detecting RFI with higher resolution utilizing DL-based architecture. We frame the RFI detection problem as a binary classification problem for each time-frequency bin. Simulated RFI types have been added to no-RFI antenna count spectrograms. The proposed DL-based detection model is trained on this synthetic dataset to detect RFI at each time-frequency bin. This framework will illustrate how different RFI types, such as pulsed or sinusoidal, chirp, and wireless communication waveforms are detected at various signal-to-noise ratio (SNR) levels. In future studies, the developed framework will be tested to understand the capability of active-passive spectrum co-existence. [4].

The remainder of the paper is organized as follows: signal model is detailed in Section 2, while the methodology for RFI detection is in Section 3. Results and discussions are provided in Section 4 and finally, a conclusion is drawn in Section 5.

This work was supported by National Science Foundation under Grant No. 2030291 and 2047771.

2. SIGNAL MODEL

2.1. Radiometer Signal Model With and Without RFI

To develop a learning-based RFI detection model, it is critical to have samples contaminated by RFI and measurements that are not affected by unwanted signals. Natural emissions from the Earth (i.e., thermal noise) can be modeled as usually distributed Gaussian noise with zero mean and variance equivalent to the noise power. Measurements are converted into IQ samples to model what is received on the radiometer receiver side. Considering a Nyquist rate of 96 MHz bandwidth for radiometer sampling and 9.6 ms of the integration period, there will be M=921600 samples. These measurements are considered to develop a SMAP-like data structure that has an exact sampling and integration period [1].

Received IQ samples on the radiometer side when there is no-RFI can be modeled as

$$x[n] = \sqrt{\frac{P_n}{2}} [I(n) + Q(n)],$$

$$n = 0, 1, \dots, M - 1$$
(1)

where $I(n) \sim \mathcal{N}(0, 1)$ and $Q(n) \sim \mathcal{N}(0, 1)$ are independent random variables, P_n corresponds to the total received noise power in the radiometer integration period. Here $\mathcal{N}(0, 1)$ refers to the standard normal random variable with zero mean and unit variance that consists of M samples.

Radiometer measurements in the presence of RFI can be written as [5]

$$y[n] = x[n] + r[n] \tag{2}$$

where x[n] is the Earth emission when there is no-RFI and r[n] is the RFI contamination in radiometer measurements. The duty cycle of the unwanted signal can be considered as $d=\frac{m}{M}$.

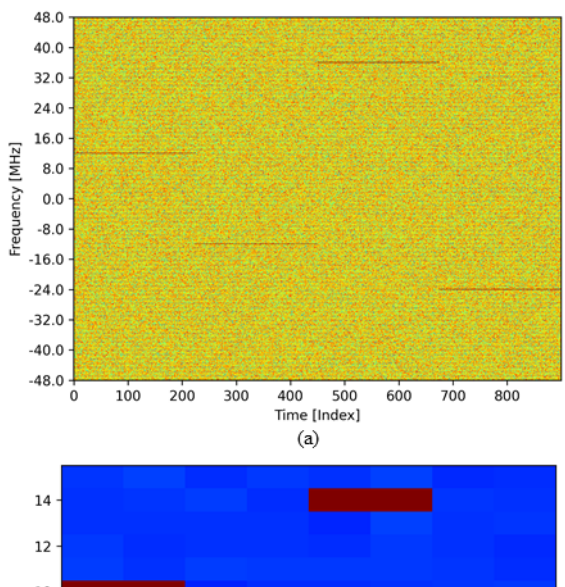
RFI sources contemplated in the study are pulsed/sinusoidal signals, chirp, and wireless communication waveforms. Pulse RFI can help to portray in-band illegal transmission in a particular time-frequency bin. Chirp and wireless communication waveforms will provide the continuous-wave nature of the RFI. This study will be conducted considering in-band illegal transmission. However, out-of-band emissions will also be modeled for future studies.

2.2. Domain Transformation

Radiometer measurements are converted into time-frequency analysis utilizing a short-time Fourier transform (STFT). Total M samples are divided into smaller blocks to perform Fourier transform to complete the domain transformation of the radiometer measurements. STFT is performed by the following equation [6]

$$STFT\{y[n]\} = Y(\omega, k) = \sum_{n = -\infty}^{\infty} x[n]w[n - m]e^{-j\omega n}$$
 (3)

where Fast Fourier Transform (FFT) is performed in a particular segment of the measurement by means of sliding window



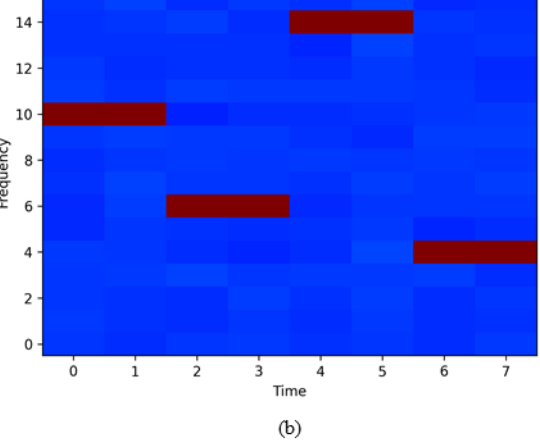


Fig. 1: Spectrograms of radiometer measurements (a) High Resolution (b) Coarse Resolution

w[n]. For this study, FFT length was selected as 1024, and a particular section has the same amount of measurements. This leads each sample of radiometer measurements with 900 columns and 1024 rows. By taking the squared magnitude of STFT, spectrograms can be generated as in

$$Spectrogram\{Y(\omega, k)\} = |Y(\omega, k)|^2$$
 (4)

This domain transformation helps to accommodate time-frequency features to the DL architecture. However, high-resolution spectrograms achieved in equations (3) and (4) might prove computationally heavy and will not be similar to the SMAP data structure. To reduce computational complexity and be comparable with an active space mission data product SMAP, this study has converted the high-resolution spectrograms into coarse spectrograms with a reduced dimension $8(time) \times 16(frequency)$. In Fig. 1, the spectrogram of a pulsed RFI-contaminated sample has been illustrated. Fig. 1b, illustrates the 16×8 structure and the primary reason for doing this is to simulate SMAP data structure. Future studies will aim to incorporate this information with SMAP level 1A and level 1B data products to verify the algorithm in various

temporal and spatial resolutions. To help with detection by aggregating more features, higher-order raw moments have also been measured that have been proven in previous studies [2]. The j-th order moment spectrograms is given as in (5)

$$Y_{i}(\omega, k) = |Y(\omega, k)|^{j} \tag{5}$$

where $Y(\omega,k)$ is the STFT derived in equation 3. Higher-order raw moments are accommodated with a 4-channel configuration at the input of the detection framework.

2.3. Spectrogram Labeling

After generating the spectrograms, we need to label the time-frequency bins as RFI or no-RFI. The portions that RFI contaminates are labeled by comparing the SNR of the sources. Each bin of 8×16 spectrograms is analyzed with a hypothesis, and an RFI map is developed that consists of "1" and "0". This is illustrated in Fig. 2. If SNR in a particular bin is above a particular threshold, then it is labeled as RFI ("1"), and the opposite leads to a no-RFI ("0") scenario. This helps to map the information of 128 pixels in a specific spectrogram to develop a multi-label classification problem.

3. METHODOLOGY

3.1. Training and Developing of DL Architecture

In computer vision, DL has successfully detected and classified objects by learning directly from the data. This study utilizes a similar kind of architecture to detect RFI within a spectrogram. Identifying the pixels or time-frequency bins in a spectrogram, whether these are contaminated by RFI or not, will be very comparable to multi-label classification problems in computer vision. In multi-label classification architecture, datasets have multiple objects within an image, which are segmented and properly labeled for further training and testing. Previous sections of this study illustrated similar samples where RFI and no-RFI pixels in a spectrogram are properly labeled.

Fig. 3 demonstrated the training of DL architecture where the input spectrogram has a dimension of $16 \times 8 \times 4$. Four-channel spectrograms make room for the higher-order moments that helps in accumulating features of RFI for training. DL architecture has four convolutional layers, each having a 3×3 kernel with 16, 32, 64, and 128 filers, respectively. Learned features from the convolutional layers are

Table 1: Performance Metrics (%) for RFI detection

SNR Levels	Accuracy	Precision	Recall	F1- Score
20	99.80	99.22	99.41	99.31
10	99.70	99.13	99.32	99.23
0	99.45	98.87	99.13	99.03
-10	97.70	97.72	97.93	97.84
-20	95.30	95.63	95.87	95.75

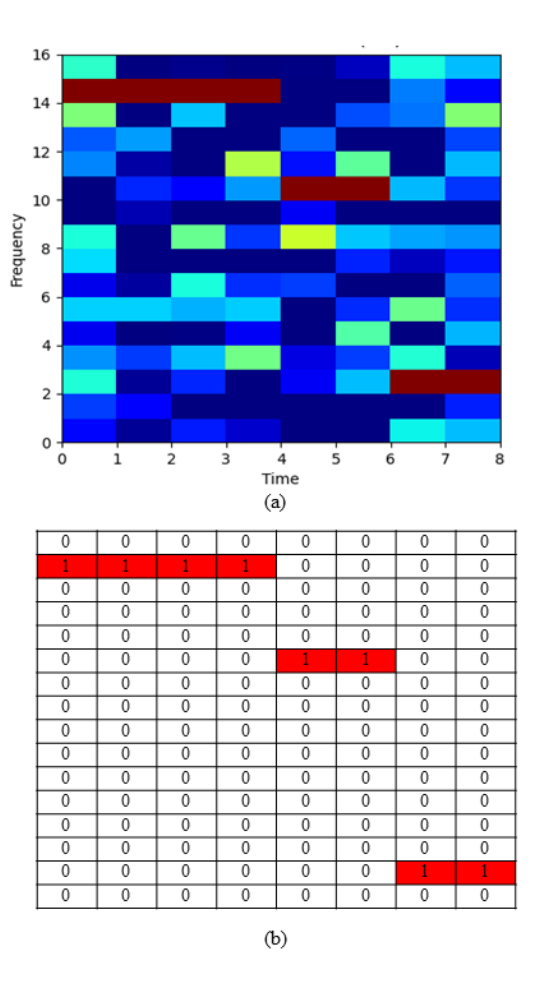


Fig. 2: Labeling of spectrograms (a) RFI contaminated samples (b) developed RFI map

fully connected (FC) with 256 neurons dense layer. The final layer consists of 128 neurons to project the probability of RFI location in each bin (i.e., $16 \times 8 = 128$). All the layers are equipped with a ReLU activation function except the final layer, which has softmax activation. During training, the predicted outcome from the DL architecture is compared with true labels that are RFI maps. The losses are measured with binary cross-entropy with the help of adam optimizer. Employing backpropagation, the model parameters are constantly updated until convergence. The model is trained with 50 epochs and 32 batch sizes.

3.2. Performance Metrics

Performance metrics are crucial in a learning-based framework to evaluate performance in terms of robustness and generalization capability. The overall dataset has been divided into 80% training and 20% testing. The testing dataset is assessed with performance metrics such as accuracy, precision, recall, and F1-score. Accuracy helps to understand the overall performance. Precision and recall help to understand false positives and missed detections.

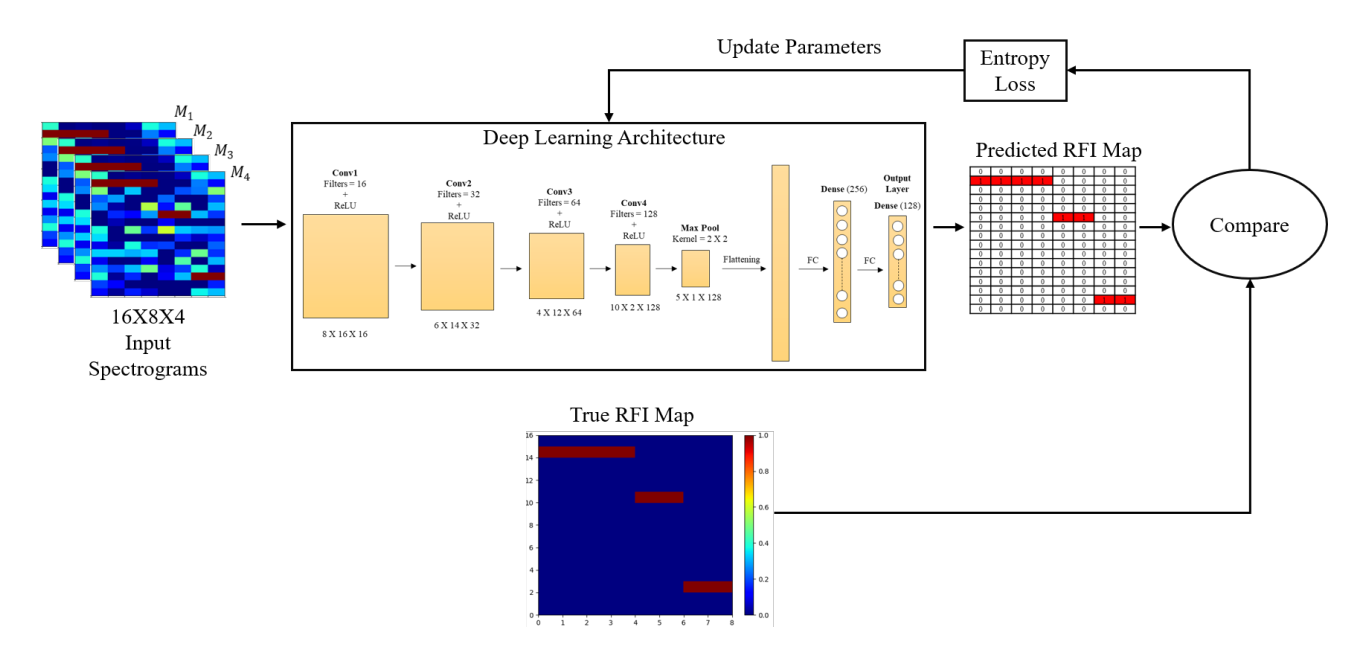


Fig. 3: Training of DL framework for high-resolution RFI detection

4. RESULTS AND DISCUSSION

4.1. Effects of SNR Levels

The performance of the testing dataset has been shown in Table 1. This analysis has been conducted in terms of SNR levels of RFI sources. SNR values range from -20 dB to 20 dB to illustrate low, medium, and higher-level RFI. Analysis shows that DL architecture proves to be very useful in locating RFI-contaminated pixels within a spectrogram. However, performance is superior during detecting high-level RFI but metrics show inferior performance at lower SNR levels. This is an indication that more care needs to be taken during low-power RFI sources which still can affect the performance of microwave radiometry.

5. CONCLUSION

This study demonstrates that DL can be utilized to detect RFI within a spectrogram which will help to preserve the non-contaminated portions in a measurement. Previous studies in DL-based RFI detection were able to identify whether RFI is present in the whole spectrogram or not. But this study can be seen as a basis for future microwave radiometry, where learning-based models can detect RFI with higher resolution. In the next iterations, authors will try to implement this study in satellite data products to understand the robustness of the algorithm.

6. REFERENCES

 J. R. Piepmeier, J. T. Johnson, P. N. Mohammed,
 D. Bradley, C. Ruf, M. Aksoy, R. Garcia, D. Hudson,
 L. Miles, and M. Wong, "Radio-frequency interference mitigation for the soil moisture active passive microwave

- radiometer," *IEEE Transactions on Geoscience and Remote Sensing*, vol. 52, no. 1, pp. 761–775, jan 2014.
- [2] A. M. Alam, M. Kurum, and A. C. Gurbuz, "Radio frequency interference detection for smap radiometer using convolutional neural networks," *IEEE Journal of Selected Topics in Applied Earth Observations and Remote Sensing*, vol. 15, pp. 10099–10112, 2022.
- [3] A. M. Alam, A. C. Gurbuz, and M. Kurum, "Smap radiometer rfi prediction with deep learning using antenna counts," in *IGARSS* 2022 - 2022 IEEE International Geoscience and Remote Sensing Symposium, 2022, pp. 8016– 8019.
- [4] Mohammad Koosha and Nicholas Mastronarde, "Opportunistic temporal spectrum coexistence of passive radiometry and active wireless networks," in 2022 IEEE Western New York Image and Signal Processing Workshop (WNYISPW), 2022, pp. 1–4.
- [5] S. Misra, P. N. Mohammed, B. Guner, C. S. Ruf, J. R. Piepmeier, and J. T. Johnson, "Microwave radiometer radio-frequency interference detection algorithms: A comparative study," *IEEE Transactions on Geoscience and Remote Sensing*, vol. 47, no. 11, pp. 3742–3754, 2009.
- [6] D. Griffin and Jae Lim, "Signal estimation from modified short-time fourier transform," *IEEE Transactions on Acoustics, Speech, and Signal Processing*, vol. 32, no. 2, pp. 236–243, 1984.